Edge Detection from Two-Dimensional Fourier Data using Gaussian Mollifiers

Anne Gelb Guohui Song Aditya Viswanathan Yang Wang

February 8, 2016

Abstract

This paper discusses the detection of edges from two-dimensional truncated Fourier spectral data. Compared to edge detection from pixel data, this is a more challenging problem since we seek accurate *local* information from a small number of often noisy *global* measurements. We propose a highly effective algorithm using a specific class of spectral mollifiers which converges *uniformly* to sharp peaks along the singular support of the function. We provide theoretical guarantees and numerical simulations to show that the resulting edge map is free of spurious edges and oscillations.

1 Introduction

The detection of jump discontinuities in piece-wise smooth functions is an important task in several areas of science and engineering. For example, many image and video processing operations such as segmentation and feature extraction rely on the accurate identification of edges in the underlying image (see for example [1, Chapter 10] for a discussion). Similarly, high-order methods for the numerical solution of PDEs often incorporate jump information when the solution is piece-wise smooth [2, Chapter 9]. Although edge detection is a non-trivial problem (especially when dealing with discrete and/or quantized data, and in the presence of noise), efficient and accurate algorithms such as the (W)ENO schemes, [3, 4] and the Canny edge detector, [5] exist for identifying edge locations when we start with *physical* space or *pixel* data. Certain applications, however, require that we extract edge information starting with *spectral* data. The most common example is magnetic resonance imaging (MRI), where the underlying physics of nuclear magnetic resonance implies that the MR scanner collects samples of the Fourier transform of the specimen being imaged. Identifying edges from such data is a significantly more challenging problem since we seek accurate *local* information from a small number of often noisy *global* measurements.

We begin by illustrating this problem in one dimension. Consider the piece-wise smooth test

function $f : [0, 1) \to \mathbb{R}$

$$f(x) = a(x)\sin(\pi x), \quad a(x) = \begin{cases} \frac{1}{2} & x \in \left[0, \frac{1}{4}\right) \\ 0 & x \in \left[\frac{1}{4}, \frac{1}{2}\right) \\ 1 & x \in \left[\frac{1}{2}, \frac{3}{4}\right) \\ -1 & x \in \left[\frac{3}{4}, 1\right). \end{cases} \tag{1.1}$$

The jump discontinuities in f are completely described by its associated *jump function*, $[f]$, defined as

$$[f](x) := \begin{cases} f(x^+) - f(x^-) & x \in (0, 1) \\ f(0^+) - f(1^-) & x = 0. \end{cases} \tag{1.2}$$

Given the first $2N + 1$ Fourier coefficients of f,

$$\hat{f}(k) = \int_0^1 f(x)e^{-2\pi ikx}dx, \quad k = -N, \ldots, N,$$

how do we identify the locations and values of its jump discontinuities, i.e., how do we approximate $[f]$? The naive approach would be to compute the $2N + 1$ mode Fourier partial sum approximation of f on an equispaced grid

$$S_N f(x_j) = \sum_{|k| \le N} \hat{f}(k)e^{2\pi ikx_j}, \quad x_j = \frac{j}{N}, \, j = 0, \ldots, N - 1,$$

followed by the application of a local differencing scheme such as the (undivided) forward difference operator

$$D_+ S_N f(x_j) = \begin{cases} S_N f(x_{j+1}) - S_N f(x_j) & j \in [0, N - 2] \\ S_N f(x_0) - S_N f(x_{N-1}) & j = N - 1. \end{cases} \tag{1.3}$$

The results using such an approach are shown in Fig. 1a, where $f, S_N f$ and $D_+ S_N f$ are plotted using dashed, solid (red) and solid(blue) lines respectively. A simple detector function of the form

$$\mathcal{E}(x_j) = \begin{cases} D_+ S_N f(x_j) & |D_+ S_N f(x_j)| > \left|D_+ S_N f(x_{(j\pm1)})\right|, \; D_+ S_N f(x_j) > \gamma \\ 0 & \text{else,} \end{cases} \tag{1.4}$$

is used to extract jump information from $D_+ S_N f$, where γ is a detection threshold. Since $S_N f$ (and consequently, $D_+ S_N f$) is a Fourier approximation of a piece-wise smooth function, it suffers from non-physical Gibbs oscillations. The largest of these (which are 9% of the corresponding jump height) are observed to be of the same order of the smallest jump in Fig. 1a. Unsurprisingly, the detector function (1.4) mistakes these oscillations for legitimate edges. Therefore, the challenge in detecting jump discontinuities from Fourier data is to distinguish these non-physical Gibbs oscillations from legitimate edges, or, to eliminate them entirely.

The latter approach was pursued by Cochran et. al. in [6], where the detection of jump discontinuities from one-dimensional truncated Fourier data using a special class of spectral

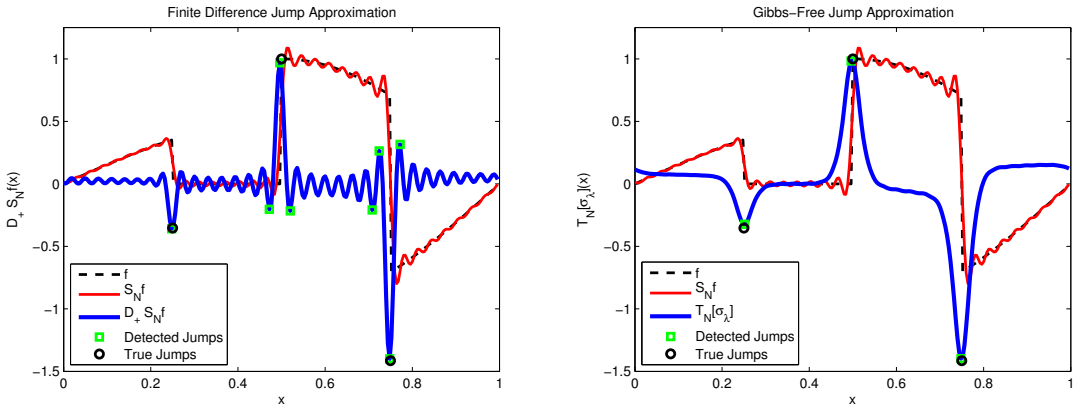

(a) (Undivided) Finite Differences

(b) Spectral Mollifiers

Figure 1: Jump Detection from one-dimensional truncated Fourier data. The jumps in test function (1.1) are detected using $2N+1$ Fourier modes, with $N = 32$ and a reconstruction grid of 250 points.

mollifiers was discussed. They proposed to approximate $[f]$ by a sequence of smooth pulses, $Q_N^\sigma(x) = \sum_{\xi\in\mathcal{K}} [f](\xi)\sigma_N(x-\xi)$, where $\mathcal{K}$ is the set of jump locations of f. For increasing N, Q_N^σ is increasingly concentrated at the jumps and σ is drawn from an appropriate class of functions so as to ensure Q_N^σ has no oscillations. Further, it was shown that a mollified Fourier derivative operator of the form

$$T_N[\sigma_{\lambda_N}](x) = 2\pi i \sum_{|k|\le N} k\,\widehat{\sigma_{\lambda_N}}(k)\,\hat{f}(k)e^{2\pi ikx} \tag{1.5}$$

converges uniformly to Q_N^σ for suitable choice of σ and sequence λ_N. A representative result of this method is shown in Fig. 1b, confirming the oscillation-free approximation qualities of $T_N[\sigma_{\lambda_N}]$. The edge detector function (1.4) applied to $T_N[\sigma_{\lambda_N}]$ now contains no spurious responses as was the case in Fig. 1a. We note that the jump approximation (1.5) is a specialization of the more general class of *concentration* edge detectors first introduced by Gelb and Tadmor in [7,8] and refined in [9–11]. These methods generally begin with a jump approximation of the form

$$S_N^\sigma[f](x) = 2\pi i \sum_{|k|\le N} \omega\left(\frac{k}{N}\right)\hat{f}(k)e^{2\pi ikx}, \tag{1.6}$$

where ω defines a *concentration factor*. The corresponding physical-space *concentration kernels* are typically odd, suitably scaled, smooth and *oscillatory*. The oscillatory nature of these kernels makes it difficult to implement reliable edge detector functions, especially in the presence of noise.

Needless to say, the same issues exist in two dimensions, as illustrated in Fig. 2, where the edges of a Shepp-Logan brain phantom are identified using the Canny edge detector. A Fourier partial sum reconstruction on a 256×256 grid and using 50×50 Fourier modes serves as the input to the Canny edge detector. Fig. 2b plots the generated edge map while Fig. 2c shows a cross-section at the center of the image. The identified edges and the Fourier reconstruction along this cross-section are plotted using dashed and solid lines respectively. The comments and

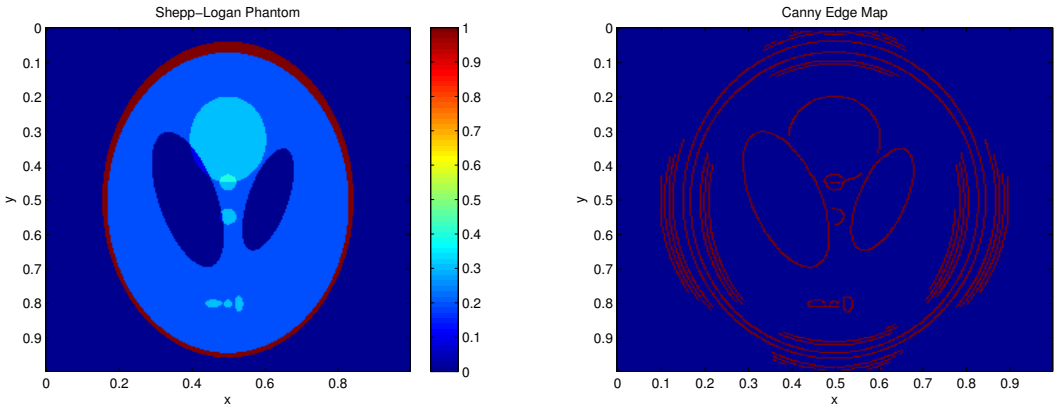

(a) Shepp-Logan Phantom

(b) Edge Map

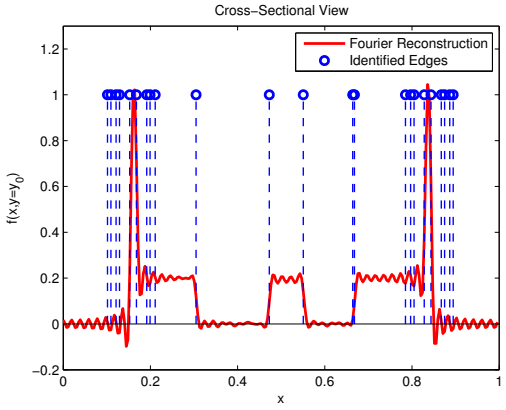

(c) Cross-Section

Figure 2: The Canny edge detector applied to a 50×50 mode partial sum Fourier reconstruction of the Shepp-Logan phantom on a 256×256 grid.

observations regarding the Gibbs phenomena in Fig. 1 apply here too. Our objective in this paper is to extend the one-dimensional framework introduced in [6] to the detection of edges from two-dimensional truncated and noisy Fourier data.

It is appropriate at this point to mention other related approaches to this problem and their relative advantages and disadvantages. We start with popular pixel-space edge detectors such as the Sobel, Prewitt or Marr-Hildreth edge detectors (see [1, Chapter 10] for a review) as well as more specialized algorithms such as the Canny edge detector [5]. As mentioned previously, these pixel- space approaches suffer from the tendency to mistake Gibbs oscillations for edges when applied to Fourier data. The method proposed here is more closely related to the two-dimensional *concentration kernel* approaches discussed in [12] and [13]. [12] uses statistical hypothesis testing methods to distinguish true edges from Gibbs oscillations, while [13] uses regularized bump functions and rotation-based post-processing operations to identify edges. The main contribution of this paper is the use of a specific form of spectral mollifier (and associated parameters) as well as a rigorous analysis of the same, demonstrating the oscillation-

free nature of the resulting edge approximation. We note that this framework can be combined with any other post-processing procedures, including Canny-type hysteresis edge tracking.

The rest of this paper is organized as follows: §2 introduces our two-dimensional edge detection scheme. A rigorous analysis examining the convergence of the scheme and confirming the absence of oscillaitons in the approximation is presented §3. §4 provides numerical results, including comparisons to pixel data methods such as the Canny edge detector and existing Fourier data schemes such as the concentration method. Performance in the presence of noise is also examined. Some concluding remarks and future directions are presented in §5.

2 Two Dimensional Edge Detection using Gaussian Mollifiers

We first give a brief introduction to the problem of detecting edges from 2-D Fourier data. Suppose $f : \mathbb{R}^2 \to \mathbb{R}$ is a piece-wise smooth and compactly supported on $[0, 1]^2$. We are given its finite Fourier data: $\hat{f}(\boldsymbol{z})$ for $\boldsymbol{z} = (z_1, z_2) \in S_N := [-N, N]^2 \cap \mathbb{Z}^2$, where

$$\hat{f}(\boldsymbol{z}) = \int_{(x,y)\in\mathbb{R}^2} f(x, y)\mathrm{e}^{-2\pi i z_1 x}\mathrm{e}^{-2\pi i z_2 y}dxdy.$$

We would like to identify all of its discontinuities in $[0, 1]^2$ and the corresponding jump heights that will be defined below.

We next present some assumptions on the function f and define the jump heights at the discontinuities. We will assume the set Γ of all the discontinuities consists of a few finite and disjoint smooth curves. In particular, we could write all the discontinuities in the following two ways:

$$(\alpha_j(y), y), \quad j = 1, 2, \ldots, N_y, \quad , y \in \mathbb{R},$$

and

$$(x, \bar{\alpha}_j(x)), \quad j = 1, 2, \ldots, M_x, \quad x \in \mathbb{R},$$

where N_y is a finite number for all but finitely many y's and M_x is a finite number for all but finitely many x's. We would also assume M_x and N_y are uniformly bounded for all $x \in \mathbb{R}$ and all $y \in \mathbb{R}$. A simple illustration is shown in Figure 3. Since we assume the discontinuities are smooth curves, both $\alpha_j(y)$ and $\bar{\alpha}_j(x)$ are smooth functions locally by the Implicit Function Theorem for almost all y's and for almost all x's respectively. Let f_x and f_y denote the partial derivatives of f at points other than the discontinuities. Note that both f_x and f_y are again piece-wise smooth with the same discontinuities of f. Let

$$[f]_1(x, y) = f(x+, y) - f(x-, y), \quad \text{and} \quad [f]_2(x, y) = f(x, y+) - f(x, y-), \quad (x, y) \in \mathbb{R}^2.$$

We point out that when they are different, one of them must be zero. In particular, $[f]_1(\alpha_j(y), y) = [f]_2(\alpha_j(y), y)$ for all but y's with $\alpha_j'(y) = 0$ or ∞. Consequently, we define the jump height $[f](x, y)$ be either one of them when they are the same, and the nonzero one if they are different.

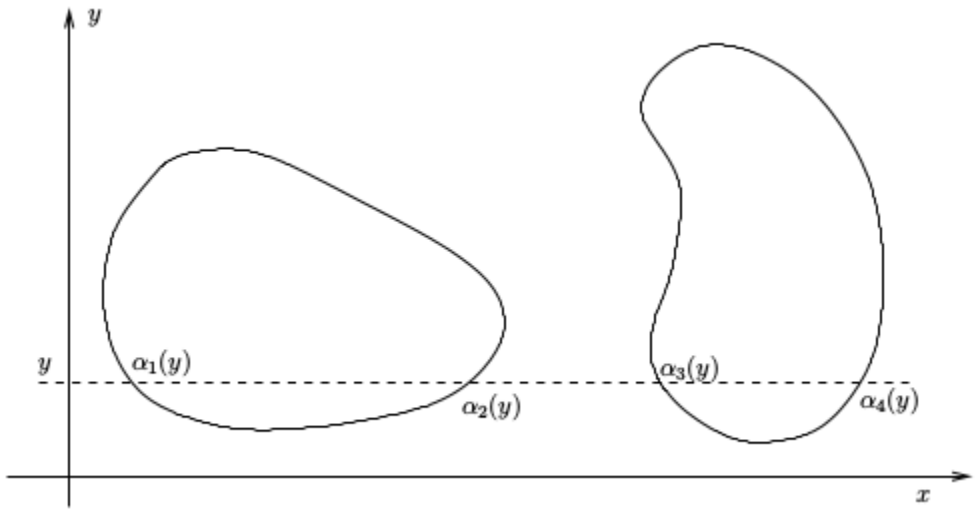

Figure 3: Edge Detection in two dimensions — Principle

We next introduce our edge detector by using the spectral Gaussian mollifiers. For $\lambda > 0$, we define

$$I_{N,\lambda}(x,y) = -2\pi i \sum_{\boldsymbol{z}\in S_N} \hat{f}(\boldsymbol{z}) z_1 \mathrm{e}^{-\frac{\|\boldsymbol{z}\|^2}{\lambda^2}} \mathrm{e}^{2\pi i(z_1 x + z_2 y)} \tag{2.1}$$

and

$$J_{N,\lambda}(x,y) = -2\pi i \sum_{\boldsymbol{z}\in S_N} \hat{f}(\boldsymbol{z}) z_2 \mathrm{e}^{-\frac{\|\boldsymbol{z}\|^2}{\lambda^2}} \mathrm{e}^{2\pi i(z_1 x + z_2 y)}.$$

We will use the following function to detect the edges of f:

$$E_{N,\lambda}(x,y) = \frac{1}{\sqrt{\pi}\lambda} \left[I_{N,\lambda}^2(x,y) + J_{N,\lambda}^2(x,y) \right]^{1/2} \mathrm{sgn}(I_{N,\lambda}(x,y)), \quad (x,y) \in \mathbb{R}^2, \tag{2.2}$$

where $\mathrm{sgn}(t) = 1$ if $t \geq 0$ and $\mathrm{sgn}(t) = -1$ otherwise.

We remark that without the Gaussian mollifier (i.e., $\lambda = \infty$), $I_{N,\lambda}(x,y)$ and $J_{N,\lambda}(x,y)$ would reduce to the partial derivatives of $f(\boldsymbol{x})$, which would yield spikes at the edges in addition to non-physical Gibbs oscillations in their vicinity. We will show in next section that with suitably chosen λ, the function $E_{N,\beta}(x,y)$ in (2.2) is a robust and accurate edge detector.

3 Convergence Analysis

We will present in this section the convergence analysis of the edge detector $E_{N,\lambda}(x,y)$ in (2.2). Specifically, we will present how to choose the parameter λ such that

(1) When (x,y) is away from the edge curves of f, the value of $E_{N,\lambda}(x,y)$ is close to zero.

(2) When (x,y) is on the edge curves of f, the value of $E_{N,\lambda}(x,y)$ is an approximation of the jump height $[f](x,y)$.

(3) The function $E_{N,\lambda}(x,y)$ behaves like sharp "mountains" rather than some oscillated peaks around the edges. That is, the Gibbs oscillation is controlled.

(4) The edge detector $E_{N,\lambda}(x,y)$ is robust with respect to small perturbations/noises on the spectral data $\hat{f}(\boldsymbol{z})$.

We point out that the convolution of f and a Gaussian function is an important resource for locating the edges of f, since the partial derivatives of the convolution would show some singular behaviors (sharp "mountains") around the edges. To this end, we would define this convolution and study the relation between its partial derivatives and our edge detector. We consider the following Gaussian function

$$\phi(x,y) = \pi \mathrm{e}^{-\pi^2(x^2+y^2)}, \quad (x,y) \in \mathbb{R}^2,$$

and for $\lambda \in \mathbb{R}$, let

$$\phi_\lambda(x,y) = \lambda^2 \phi(\lambda x, \lambda y), \quad (x,y) \in \mathbb{R}^2. \tag{3.1}$$

We then convolve f with ϕ_λ:

$$F_\lambda(x,y) = (f * \phi_\lambda)(x,y) = \int_{(s,t)\in\mathbb{R}^2} f(s,t)\phi_\lambda(x-s, y-t)dsdt, \quad (x,y) \in \mathbb{R}^2. \tag{3.2}$$

We will next focus on deriving estimates of the edge detector $I_{N,\lambda}$. The estimates of $J_{N,\lambda}$ could be obtained in a similar way. We shall first show a relation between $I_{N,\lambda}$ and the partial derivative $\frac{\partial F_\lambda}{\partial x}$. To this end, for $(x,y) \in \mathbb{R}^2$ we let

$$Q_\lambda(x,y) = \sum_{\boldsymbol{z}\in\mathbb{Z}^2} \frac{\partial F_\lambda(x+z_1, y+z_2)}{\partial x}, \tag{3.3}$$

and

$$B_N(x,y) = 2\pi i \sum_{\boldsymbol{z}\in\mathbb{Z}^2\setminus S_N} \hat{f}(\boldsymbol{z}) z_1 \mathrm{e}^{-\frac{\|\boldsymbol{z}\|^2}{\lambda^2}} \mathrm{e}^{2\pi i(z_1 x + z_2 y)}. \tag{3.4}$$

Proposition 3.1 *For $(x,y) \in \mathbb{R}^2$, there holds*

$$I_{N,\lambda}(x,y) = Q_\lambda(x,y) + B_N(x,y).$$

Moreover, there exists a positive constant c such that for any $(x,y) \in \mathbb{R}^2$ and $N \in \mathbb{N}$

$$|I_{N,\lambda}(x,y) - Q_\lambda(x,y)| \le c\lambda^3 \mathrm{e}^{-\frac{3N^2}{2\lambda^2}}.$$

Proof: We will prove the equality by a direct computation. To this end, we define the shift of the partial derivatives

$$g_{(x,y)}(s,t) = \frac{\partial F_\lambda(x+s, y+t)}{\partial x}, \quad (s,t) \in \mathbb{R}^2.$$

It follows that

$$Q_\lambda(x,y) = \sum_{\boldsymbol{z}\in\mathbb{Z}^2} g_{(x,y)}(\boldsymbol{z}).$$

On the other hand, a direct computation yields that $\hat{g}_{(x,y)}(\boldsymbol{\xi}) = -2\pi i \hat{f}(\boldsymbol{\xi})\xi_1 \mathrm{e}^{-\frac{\|\boldsymbol{\xi}\|^2}{\lambda^2}} \mathrm{e}^{2\pi i(\xi_1 x+\xi_2 y)}$. By the Poisson summation formula,

$$Q_\lambda(x,y) = \sum_{\boldsymbol{z}\in\mathbb{Z}^2} \hat{g}_{(x,y)}(\boldsymbol{z}) = \sum_{\boldsymbol{z}\in\mathbb{Z}^2} -2\pi i \hat{f}(\boldsymbol{z})\xi_1 \mathrm{e}^{-\frac{\|\boldsymbol{z}\|^2}{\lambda^2}} \mathrm{e}^{2\pi i(z_1 x+z_2 y)}$$

This combined with the definition of $I_{N,\beta}$ in (2.1) and the definition of B_N in (3.4) implies the desired equality.

We next show the inequality. It is enough to show $B_N(x,y)$ is bounded by the right hand side of the inequality. Since $f \in L^2[0,1]$, there exists a positive constant c_0 such that $|\hat{f}(\boldsymbol{z})| \le c_0$. It follows from (3.4) that

$$|B_N(x,y)| \le 2\pi c_0 \sum_{\boldsymbol{z}\in\mathbb{Z}^2\setminus S_N} z_1 \mathrm{e}^{-\frac{\|\boldsymbol{z}\|^2}{\lambda^2}} = 2\pi c_0 \sum_{z_1>N} z_1 \mathrm{e}^{-\frac{z_1^2}{\lambda^2}} \sum_{z_2>N} \mathrm{e}^{-\frac{z_2^2}{\lambda^2}}.$$

It is direct to observe that $\sum_{z_1>N} z_1 \mathrm{e}^{-\frac{z_1^2}{\lambda^2}} \le \int_N^\infty t\mathrm{e}^{-\frac{t^2}{\lambda^2}} dt = \frac{\lambda^2}{2}\mathrm{e}^{-\frac{N^2}{\lambda^2}}$. Moreover, by using the polar coordinates, it follows from a direct computation that $\sum_{z_2>N} \mathrm{e}^{-\frac{z_2^2}{\lambda^2}} \le \frac{\sqrt{\pi}}{2}\lambda \mathrm{e}^{-\frac{N^2}{2\lambda^2}}$. Substituting these two estimates into the above inequality, we have

$$|B_N(x,y)| \le \frac{\pi^{3/2}}{2} c_0 \lambda^3 \mathrm{e}^{-\frac{3N^2}{\lambda^2}},$$

which implied the desired inequality. □

We point out that we could choose appropriate λ depending on N such that $B_N(x,y)$ converges to zero uniformly, which avoids the Gibbs oscillation in the edge detectors. More details will be shown in later results.

We shall next analyze the behavior of Q_λ. In particular, we will show that Q_λ has peaks at the edges by using its relation with the partial derivative $\frac{\partial F_\lambda}{\partial x}$. To this end, we first present a direct computation of $\frac{\partial F_\lambda}{\partial x}$. We let

$$\tilde{I}_\lambda(x,y) = \int_{\mathbb{R}} \sum_{j=1}^{N_t} [f]_1(\alpha_j(t),t)\, \phi_\lambda(x-\alpha_j(t), y-t) dt, \tag{3.5}$$

and

$$H_\lambda(x,y) = \int_{(s,t)\in\mathbb{R}^2} f_x(s,t)\phi_\lambda(x-s,y-t) ds dt. \tag{3.6}$$

We have the following result of the partial derivative $\frac{\partial F_\lambda}{\partial x}$.

Proposition 3.2 *For any $(x,y) \in \mathbb{R}^2$, there holds that*

$$\frac{\partial F_\lambda}{\partial x}(x,y) = \tilde{I}_\lambda(x,y) + H_\lambda(x,y).$$

Moreover, if the edge curves are at least ϵ away from the boundary of $[0,1]^2$, that is, $\sqrt{(x-x^*)^2+(y-y^*)^2} \geq \epsilon$ for all $(x,y) \in [0,1]^2$ with either $x \in \{0,1\}$ or $y \in \{0,1\}$ and for all (x^*,y^*) on the edge curves, then there exists a positive constant c such that for $(x,y) \in [0,1]^2$

$$|Q_\lambda(x,y) - \tilde{I}_\lambda(x,y)| \leq c\pi\lambda^2 \mathrm{e}^{-\pi^2\lambda^2\epsilon^2} + c\pi\lambda^2 \frac{\mathrm{e}^{-\pi^2\lambda^2}}{(1-\mathrm{e}^{-\pi^2\lambda^2})^2} + \|f_x\|_\infty.$$

Proof: We first show the equality about the decomposition of $\frac{\partial F_\lambda}{\partial x}$. From the definition of ∂F_λ in (3.2), we have

$$\frac{\partial F_\lambda}{\partial x}(x,y) = \int_{(s,t)\in\mathbb{R}^2} f(s,t) \frac{\partial \phi_\lambda}{\partial x}(x-s, y-t) ds dt.$$

A direct calculation of $\frac{\partial \phi_\lambda}{\partial x}$ from (3.1) yields that

$$\frac{\partial F_\lambda}{\partial x}(x,y) = \lambda^3 \int_{t\in\mathbb{R}} \left[\int_{s\in\mathbb{R}} f(s,t) \phi_x(\lambda(x-s), \lambda(y-t)) ds \right] dt.$$

Note that for $t \in \mathbb{R}$, $f(\cdot,t)$ has discontinuities $\alpha_j(t)$ for $1 \leq j \leq N_t$. For simplicity of presentation, we let $\alpha_0(t) = -\infty$ and $\alpha_{N_t+1}(t) = \infty$. It follows that

$$\frac{\partial F_\lambda}{\partial x}(x,y) = \lambda^3 \int_{t\in\mathbb{R}} \left[\sum_{j=1}^{N_t+1} \int_{\alpha_{j-1}(t)}^{\alpha_j(t)} f(s,t) \phi_x(\lambda(x-s), \lambda(y-t)) ds \right] dt.$$

Apply integration by parts and we have

$$\frac{\partial F_\lambda}{\partial x}(x,y) = \lambda^2 \int_{t\in\mathbb{R}} \left[-\sum_{j=1}^{N_t+1} f(s,t) \phi(\lambda(x-s), \lambda(y-t)) \Big|_{\alpha_{j-1}(t)}^{\alpha_j(t)} + \int_{\mathbb{R}} f_x(s,t) \phi(\lambda(x-s), \lambda(y-t)) ds \right] dt.$$

The desires equality follows from a direct calculation from the above equality.

We next estimate the difference of $Q_\lambda(x,y)$ and $\tilde{I}_\lambda(x,y)$. It follows from the definition of Q_λ in (3.3) and the equality shown above that

$$|Q_\lambda(x,y) - \tilde{I}_\lambda(x,y)| \leq \sum_{\boldsymbol{z}\neq 0} |\tilde{I}_\lambda(x+z_1, y+z_2)| + \sum_{\boldsymbol{z}\in\mathbb{Z}^2} |H_\lambda(x+z_1, y+z_2)|. \tag{3.7}$$

We will estimate the two terms in the right hand side of the above inequality separately.

We start with an estimate of first term. Note that both N_t and $[f]_1(\lambda_j(t), t)$ are uniformly bounded for all t. It follows from the definition of $\tilde{I}_\lambda$ in (3.5) that there exists a positive constant c_0 such that

$$\sum_{\boldsymbol{z}\neq 0} |\tilde{I}_\lambda(x+z_1, y+z_2)| \leq c_0 \sum_{\boldsymbol{z}\neq 0} \int_{\mathbb{R}} \phi_\lambda(x+z_1-\alpha_j(t), y+z_2-t) dt.$$

Note that when $\boldsymbol{z} \neq 0$, the point $(x+z_1, y+z_2)$ is not in $[0,1]^2$. By assumption, it is at least ϵ away from the edge curves. In particular, when $\boldsymbol{z} \in E := \{-1,0,1\}^2 \backslash (0,1)$, we have $\left((x+z_1-\alpha_j(t))^2 + (y+z_2-t)^2\right)^{1/2} \geq \epsilon$. On the other hand side, when $|z_1| \geq 2$, the point $(x+z_1, y+z_2)$ is at least $|z_1|-1$ away from the edge curves. When $|z_2| \geq 2$, the point

$(x+z_1, y+z_2)$ is at least $|z_2|-1$ away from the edge curves. Substituting these estimates into ϕ_λ as in (3.1) yields that

$$\begin{aligned}
&\sum_{\boldsymbol{z}\neq 0} |\tilde{I}_\lambda(x+z_1, y+z_2)| \\
\leq\ & \sum_{\boldsymbol{z}\in E} |\tilde{I}_\lambda(x+z_1, y+z_2)| + \sum_{z_1\in\mathbb{Z}, |z_2|\geq 2} |\tilde{I}_\lambda(x+z_1, y+z_2)| + \sum_{|z_1|\geq 2, z_2\in\mathbb{Z}} |\tilde{I}_\lambda(x+z_1, y+z_2)| \\
\leq\ & 5c_0\pi\lambda^2 \mathrm{e}^{-\pi^2\lambda^2\epsilon^2} + 4c_0\pi\lambda^2 \frac{1}{1-\mathrm{e}^{-\pi^2\lambda^2}} \frac{\mathrm{e}^{-\pi^2\lambda^2}}{1-\mathrm{e}^{-\pi^2\lambda^2}},
\end{aligned}$$

which combined with (3.7) implies

$$|Q_\lambda(x,y) - \tilde{I}_\lambda(x,y)| \leq 5c_0\pi\lambda^2 \mathrm{e}^{-\pi^2\lambda^2\epsilon^2} + 4c_0\pi\lambda^2 \frac{\mathrm{e}^{-\pi^2\lambda^2}}{(1-\mathrm{e}^{-\pi^2\lambda^2})^2} + \sum_{\boldsymbol{z}\in\mathbb{Z}^2} |H_\lambda(x+z_1, y+z_2)|.$$

To show the desired result on $|Q_\lambda(x,y) - \tilde{I}_\lambda(x,y)|$, it remains to prove $\sum_{\boldsymbol{z}\in\mathbb{Z}^2} |H_\lambda(x+z_1, y+z_2)| \leq \|f_x\|_\infty$. Note that $f_x(s,t) = 0$ when $(s,t) \notin [0,1]^2$. It is direct to observe from the definition of H_λ in (3.6) that for any $\boldsymbol{z} \in \mathbb{Z}^2$,

$$\begin{aligned}
|H_\lambda(x+z_1, y+z_2)| &= \left| \int_{(s,t)\in[0,1]^2} f_x(s,t)\phi_\lambda(x+z_1-s, y+z_2-t) ds dt \right| \\
&\leq \|f_x\|_\infty \int_{(s,t)\in[0,1]^2} \phi_\lambda(x+z_1-s, y+z_2-t) ds dt,
\end{aligned}$$

It implies

$$\begin{aligned}
\sum_{\boldsymbol{z}\in\mathbb{Z}^2} |H_\lambda(x+z_1, y+z_2)| &\leq \|f_x\|_\infty \sum_{\boldsymbol{z}\in\mathbb{Z}^2} \int_{(s,t)\in[0,1]^2} \phi_\lambda(x+z_1-s, y+z_2-t) ds dt \\
&= \|f_x\|_\infty \int_{(u,v)\in\mathbb{R}^2} \phi_\lambda(u,v) du dv \\
&= \|f_x\|_\infty,
\end{aligned}$$

which finishes the proof. □

We will continue with the analysis of $\tilde{I}_\lambda$. In particular, we will show that it is concentrated around the edges of f.

Proposition 3.3 *(i) When (x,y) is at least ϵ away from the edges, that is, $dist((x,y),\Gamma) \geq \epsilon$, there exists a positive constant c such that*

$$|\tilde{I}_\lambda(x,y)| \leq c\lambda^2 \mathrm{e}^{-\pi^2\lambda^2\epsilon^2}.$$

(ii) When (x^*, y^*) is on the edge, that is, $x^* = \alpha_{j_0}(y^*)$ for some $j_0 \in \mathbb{N}$, if there exists a $\epsilon > 0$ such that $d((\alpha_j(y), y), (\alpha_{j_0}(y^*), y^*)) = \sqrt{(\alpha_j(y) - \alpha_{j_0}(y^*))^2 + (y-y^*)^2} \geq \epsilon$ for all $j \neq j_0$

and $y \in [0,1]$, then there exists a positive constant c such that

$$\left|\tilde{I}_\lambda(x^*,y^*) - [f]_1(x^*,y^*)\frac{\sqrt{\pi}\lambda}{\sqrt{1+(\alpha'_{j_0}(y^*))^2}}\right| \le c\big(\lambda \mathrm{e}^{-\pi^2\lambda^2\epsilon^2} + \lambda^2\mathrm{e}^{-\pi^2\lambda^2\epsilon^2} + (\lambda\epsilon)^2 + (\lambda\epsilon)^4\big).$$

Proof: (i) Note that both N_t and the jump heights $[f]_1(\alpha_j(t),t)$ are uniformly bounded. Since f is compactly supported on $[0,1]$, it follows from the definition of tI_λ in (3.5) that there exists a positive constant c_0 such that

$$|\tilde{I}_\lambda(x,y)| \le c_0 \int_0^1 \phi_\lambda(x-\alpha_j(t), y-t)dt.$$

By the definition of ϕ_λ in (3.1),

$$|\tilde{I}_\lambda(x,y)| \le c_0 \int_0^1 \lambda^2 \mathrm{e}^{-\pi^2\lambda^2((x-\alpha_j(t))^2+(y-t)^2)}dt.$$

When $dist((x,y),\Gamma) \ge \epsilon$, that is, $(x-\alpha_j(t))^2 + (y-t)^2 \ge \epsilon^2$ for all $t \in [0,1]$,

$$|\tilde{I}_\lambda(x,y)| \le c_0\lambda^2\mathrm{e}^{-\pi^2\lambda^2\epsilon^2}.$$

(ii) By (3.5) we have that

$$\tilde{I}_\lambda(x^*,y^*) = \int_{\mathbb{R}} \sum_{j=1}^{N_t} [f]_1(\alpha_j(t),t)\,\phi_\lambda(\alpha_{j_0}(y^*) - \alpha_j(t), y^*-t)dt. \tag{3.8}$$

It follows from the same argument in (i) that

$$\int_{|t-y^*|\ge\epsilon} \sum_{j=1}^{N_t} [f]_1(\alpha_j(t),t)\,\phi_\lambda(\alpha_{j_0}(y^*) - \alpha_j(t), y^*-t)dt \le c_0\lambda^2\mathrm{e}^{-\pi^2\lambda^2\epsilon^2},$$

and

$$\int_{\mathbb{R}} \sum_{j\ne j_0} [f]_1(\alpha_j(t),t)\,\phi_\lambda(\alpha_{j_0}(y^*) - \alpha_j(t), y^*-t)dt \le c_0\lambda^2\mathrm{e}^{-\pi^2\lambda^2\epsilon^2}.$$

These two inequalities combined with (3.8) yields that

$$\left|\tilde{I}_\lambda(x^*,y^*) - \tilde{I}_{\lambda,\epsilon}(x^*,y^*)\right| \le 2c_0\lambda^2\mathrm{e}^{-\pi^2\lambda^2\epsilon^2}. \tag{3.9}$$

where

$$\tilde{I}_{\lambda,\epsilon}(x^*,y^*) = \int_{|t-y^*|\le\epsilon} [f]_1(\alpha_{j_0}(t),t)\,\phi_\lambda(\alpha_{j_0}(y^*) - \alpha_{j_0}(t), y^*-t)dt. \tag{3.10}$$

We next estimate the integral $\tilde{I}_{\lambda,\epsilon}(x^*,y^*)$. Since both $[f]_1$ and α_{j_0} are smooth functions locally, there exist positive constants c_1 and c_2 such that for $|t-y^*| \le \epsilon$

$$\big|[f]_1(\alpha_{j_0}(t),t) - [f]_1(\alpha_{j_0}(y^*),y^*)\big| \le c_1|t-y^*|, \tag{3.11}$$

and

$$|\alpha_{j_0}(t)-\alpha_{j_0}(y^*)-\alpha'_{j_0}(y^*)(t-y^*)|\le c_2|t-y^*|^2. \tag{3.12}$$

By the definition of ϕ_λ in (3.1),

$$\phi_\lambda(\alpha_{j_0}(y^*)-\alpha_{j_0}(t),y^*-t)=\pi\lambda^2\mathrm{e}^{-\pi^2\lambda^2[(\alpha_{j_0}(y^*)-\alpha_{j_0}(t))^2+(t-y^*)^2]}.$$

Since α_{j_0} is smooth, there exists a positive constant c_3 such that $|\alpha_{j_0}(t)-\alpha_{j_0}(y^*)+\alpha'_{j_0}(y^*)(t-y^*)|\le c_3|t-y^*|$. This combined with (3.12) yields that $\big|(\alpha_{j_0}(t)-\alpha_{j_0}(y^*))^2-(\alpha'_{j_0}(y^*))^2(t-y^*)^2\big|\le c_2c_3|t-y^*|^3$. Substituting it into the above equality and putting

$$\psi_\lambda(t)=\pi\lambda^2\mathrm{e}^{-\pi^2\lambda^2[1+(\alpha'_{j_0}(y^*))^2](t-y^*)^2}, \tag{3.13}$$

we have

$$\Big|\phi_\lambda(\alpha_{j_0}(y^*)-\alpha_{j_0}(t),y^*-t)-\psi_\lambda(t)\Big|\le\psi_\lambda(t)\big(1-\mathrm{e}^{-\pi^2\lambda^2c_2c_3|t-y^*|^3}\big).$$

Since $1-\mathrm{e}^{-x}\le x$ for $x\ge0$,

$$\Big|\phi_\lambda(\alpha_{j_0}(y^*)-\alpha_{j_0}(t),y^*-t)-\psi_\lambda(t)\Big|\le\psi_\lambda(t)\pi^2\lambda^2c_2c_3|t-y^*|^3.$$

We can now estimate $\tilde I_{\lambda,\epsilon}(x^*,y^*)$ as in (3.10) following from the above inequality and (3.11)

$$\begin{aligned}
&\Big|\tilde I_{\lambda,\epsilon}(x^*,y^*)-\int_{|t-y^*|\le\epsilon}[f]_1(\alpha_{j_0}(y^*),y^*)\psi_\lambda(t)dt\Big|\\
\le\ &\Big|\int_{|t-y^*|\le\epsilon}\big([f]_1(\alpha_{j_0}(t),t)-[f]_1(\alpha_{j_0}(y^*),y^*)\big)\psi_\lambda(t)dt\Big|\\
&+\Big|\int_{|t-y^*|\le\epsilon}[f]_1(\alpha_{j_0}(y^*),y^*)(\phi_\lambda(\alpha_{j_0}(y^*)-\alpha_{j_0}(t),y^*-t)-\psi_\lambda(t))dt\Big|\\
\le\ &c_1\Big|\int_{|t-y^*|\le\epsilon}|t-y^*|\psi_\lambda(t)dt\Big|+c_2c_3|[f]_1(\alpha_{j_0}(y^*),y^*)|\Big|\int_{|t-y^*|\le\epsilon}\psi_\lambda(t)\pi^2\lambda^2|t-y^*|^3dt\Big|.
\end{aligned}$$

It is direct to observe from (3.13) that $\psi_\lambda(t)\le\pi\lambda^2\mathrm{e}^{-\pi^2\lambda^2(t-y^*)^2}$. Moreover, there exists a positive constant c_4 such that $c_2c_3|[f]_1(\alpha_{j_0}(y^*),y^*)\le c_4$ for all $y^*\in[0,1]$. Substituting these into the above inequality and having a change of variable $u=t-y^*$ yields that

$$\Big|\tilde I_{\lambda,\epsilon}(x^*,y^*)-\int_{|t-y^*|\le\epsilon}[f]_1(\alpha_{j_0}(y^*),y^*)\psi_\lambda(t)dt\Big|\le2c_1\pi\lambda^2\int_0^\epsilon u\mathrm{e}^{-\pi^2\lambda^2u^2}du+2c_4\pi^3\lambda^4\int_0^\epsilon u^3\mathrm{e}^{-\pi^2\lambda^2u^2}du.$$

Since $\mathrm{e}^{-\pi^2\lambda^2u^2}\le1$ for all $u\ge0$, it follows from a direct computation of the above integrals that

$$\Big|\tilde I_{\lambda,\epsilon}(x^*,y^*)-\int_{|t-y^*|\le\epsilon}[f]_1(\alpha_{j_0}(y^*),y^*)\psi_\lambda(t)dt\Big|\le c_1\pi(\lambda\epsilon)^2+\frac{1}{2}c_4\pi^3(\lambda\epsilon)^4. \tag{3.14}$$

We next estimate the integral in the above inequality. To this end, we let $F(a) = \int_{-a}^{a} \mathrm{e}^{-x^2} dx$. A direction computation from (3.13) gives that

$$\int_{|t-y^*|\le\epsilon} \psi_\lambda(t)dt = \frac{\lambda}{\sqrt{1+(\alpha'_{j_0}(y^*))^2}} F\big(\pi\lambda\sqrt{1+(\alpha'_{j_0}(y^*))^2}\epsilon\big).$$

Note that by using the polar coordinates in the integral, we have the following estimates of $F(a)$: $\pi(1-\mathrm{e}^{-a^2}) \le F^2(a) \le \pi(1-\mathrm{e}^{-2a^2})$, which implies $|F(a) - \sqrt{\pi}| \le \sqrt{\pi}\mathrm{e}^{-a^2}$. Substituting it into the above equation, we have

$$\left|\int_{|t-y^*|\le\epsilon} \psi_\lambda(t)dt - \frac{\sqrt{\pi}\lambda}{\sqrt{1+(\alpha'_{j_0}(y^*))^2}}\right| \le \frac{\sqrt{\pi}\lambda}{\sqrt{1+(\alpha'_{j_0}(y^*))^2}} \mathrm{e}^{-\pi^2(1+(\alpha'_{j_0}(y^*))^2)\lambda^2\epsilon^2} \le \sqrt{\pi}\lambda\mathrm{e}^{-\pi^2\lambda^2\epsilon^2}.$$

Since $[f]_1$ is continuous, there exists a positive constant c_5 such that $|[f]_1(x^*, y^*)| \le c_5$ for all $y^* \in [0,1]$. It implies

$$\left|\int_{|t-y^*|\le\epsilon} [f]_1(\alpha_{j_0}(y^*), y^*)\psi_\lambda(t)dt - [f]_1(\alpha_{j_0}(y^*), y^*)\frac{\sqrt{\pi}\lambda}{\sqrt{1+(\alpha'_{j_0}(y^*))^2}}\right| \le c_5\sqrt{\pi}\lambda\mathrm{e}^{-\pi^2\lambda^2\epsilon^2}.$$

The desired result follows from this combined with (3.9) and (3.14). □

We remark that we could choose appropriate λ and ϵ such that $\tilde{I}_\lambda(x,y)$ will be arbitrarily small when the point (x,y) is away from the edge curves and it will blow up when the point (x,y) is on the edge curve. That is, $\tilde{I}_\lambda(x,y)$ behaves like a "sharp mountain" around the edge curves. We will present the specific choices of λ and ϵ in the later results.

We are now ready to present the edge detection behavior of $I_{N,\lambda}$.

Theorem 3.4 *(i) When (x,y) is at least ϵ away from the edges, that is, $dist((x,y),\Gamma) \ge \epsilon$, there exists a positive constant c such that*

$$\left|\frac{I_{N,\lambda}(x,y)}{\sqrt{\pi}\lambda}\right| \le c\bigg(\lambda^2\mathrm{e}^{-\frac{3N^2}{2\lambda^2}} + \lambda\mathrm{e}^{-\pi^2\lambda^2\epsilon^2} + \lambda\frac{\mathrm{e}^{-\pi^2\lambda^2}}{(1-\mathrm{e}^{-\pi^2\lambda^2})^2} + \frac{\|f_x\|_\infty}{\lambda}\bigg).$$

(ii) When (x^*, y^*) is on the edge, that is, $x^* = \alpha_{j_0}(y^*)$ for some $j_0 \in \mathbb{N}$, if there exists a $\epsilon > 0$ such that $d((\alpha_j(y), y), (\alpha_{j_0}(y^*), y^*)) \ge \epsilon$ for all $j \ne j_0$ and $y \in [0,1]$, then there exists a positive constant c such that

$$\left|\frac{I_{N,\lambda}(x^*,y^*)}{\sqrt{\pi}\lambda} - \frac{[f]_1(x^*,y^*)}{\sqrt{1+(\alpha'_{j_0}(y^*))^2}}\right| \le c\bigg(\lambda^2\mathrm{e}^{-\frac{3N^2}{2\lambda^2}} + \lambda\frac{\mathrm{e}^{-\pi^2\lambda^2}}{(1-\mathrm{e}^{-\pi^2\lambda^2})^2} + \frac{\|f_x\|_\infty}{\lambda} + (\lambda+1)\mathrm{e}^{-\pi^2\lambda^2\epsilon^2} + \lambda\epsilon^2 + \lambda^3\epsilon^4\bigg).$$

Proof: It follows immediately from Propositions 3.1, 3.2, and 3.3. □

Similarly, we could obtain the following estimates on $J_{N,\lambda}$.

Theorem 3.5 *(i) When (x,y) is at least ϵ away from the edges, that is, $dist((x,y),\Gamma) \ge \epsilon$,*

there exists a positive constant c such that

$$\left|\frac{J_{N,\lambda}(x,y)}{\sqrt{\pi}\lambda}\right| \le c\bigg(\lambda^2 \mathrm{e}^{-\frac{3N^2}{2\lambda^2}} + \lambda \mathrm{e}^{-\pi^2\lambda^2\epsilon^2} + \lambda\frac{\mathrm{e}^{-\pi^2\lambda^2}}{(1-\mathrm{e}^{-\pi^2\lambda^2})^2} + \frac{\|f_y\|_\infty}{\lambda}\bigg).$$

(ii) When (x^*, y^*) is on the edge, that is, $y^* = \bar{\alpha}_{l_0}(x^*)$ for some $l_0 \in \mathbb{N}$, if there exists a $\epsilon > 0$ such that $d((x, \bar{\alpha}_l(x)), (x^*, \bar{\alpha}_{l_0}(x^*))) \ge \epsilon$ for all $l \ne l_0$ and $x \in [0,1]$, then there exists a positive constant c such that

$$\left|\frac{J_{N,\lambda(x^*,y^*)}}{\sqrt{\pi}\lambda} - \frac{[f]_2(x^*,y^*)}{\sqrt{1+(\bar{\alpha}'_{l_0}(x^*))^2}}\right| \le c\bigg(\lambda^2\mathrm{e}^{-\frac{3N^2}{2\lambda^2}} + \lambda\frac{\mathrm{e}^{-\pi^2\lambda^2}}{(1-\mathrm{e}^{-\pi^2\lambda^2})^2} + \frac{\|f_y\|_\infty}{\lambda} + (\lambda+1)\mathrm{e}^{-\pi^2\lambda^2\epsilon^2} + \lambda\epsilon^2 + \lambda^3\epsilon^4\bigg).$$

Proof: It follows immediately from Propositions 3.1, 3.2, and 3.3. □

Consequently, we will present the main result of this paper below. In particular, we will show the specific choices of λ and ϵ such that the edge detector $E_{N,\lambda}$ as in (2.2) behaves like oscillation-free sharp "mountains" around the edges.

Theorem 3.6 *If $\lambda = c_0 \frac{N}{\log N}$ and $\epsilon = c_1(\frac{N}{\log N})^{-p}$ for some positive constants c_0, c_1 and $\frac{3}{4} < p < 1$, then for large enough N,*

(i) when (x,y) is at least ϵ away from the edges, that is, $dist((x,y),\Gamma) \ge \epsilon$, there exists a positive constant c such that

$$|E_{N,\lambda}(x,y)| \le c\,\frac{\log N}{N};$$

(ii) when (x^*, y^*) is on the edge, that is, $x^* = \alpha_{j_0}(y^*)$ and $y^* = \bar{\alpha}_{l_0}(x^*)$ for some $j_0, l_0 \in \mathbb{N}$, if there exists a $\epsilon > 0$ such that $d((\alpha_j(y), y), (\alpha_{j_0}(y^*), y^*)) \ge \epsilon$ for all $j \ne j_0$ and $y \in [0,1]$ and $d((x, \bar{\alpha}_l(x)), (x^*, \bar{\alpha}_{l_0}(x^*))) \ge \epsilon$ for all $l \ne l_0$ and $x \in [0,1]$, then there exists a positive constant c such that

$$\left|E_{N,\lambda}(x^*,y^*) - [f](x^*,y^*)\right| \le c\left(\frac{\log N}{N}\right)^{4p-3}.$$

Proof: (i) It follows from a direct computation from substituting the choices of λ and ϵ into Theorems 3.4, 3.5 and the definition of $E_{N,\lambda}$ in (2.2).

(ii) Note that when $x^* = \alpha_{j_0}(y^*)$ and $y^* = \bar{\alpha}_{l_0}(x^*)$, we have $[f](x^*,y^*) = [f]_1(x^*,y^*) = [f]_2(x^*,y^*)$ and $\left(\frac{1}{\sqrt{1+(\alpha'_{j_0}(y^*))^2}}\right)^2 + \left(\frac{1}{\sqrt{1+(\bar{\alpha}'_{l_0}(x^*))^2}}\right)^2 = 1$. The desired result follows immediately from a direct computation from substituting the choices of λ and ϵ into Theorems 3.4, 3.5 and the definition of $E_{N,\lambda}$ in (2.2). □

4 Numerical Results

We now present numerical results demonstrating the accuracy of the proposed formulation. Matlab code used to generate the figures in this section can be found at [14]. We begin with Figure 4, where we plot the edge map of a Shepp-Logan phantom on a 256×256 grid given its

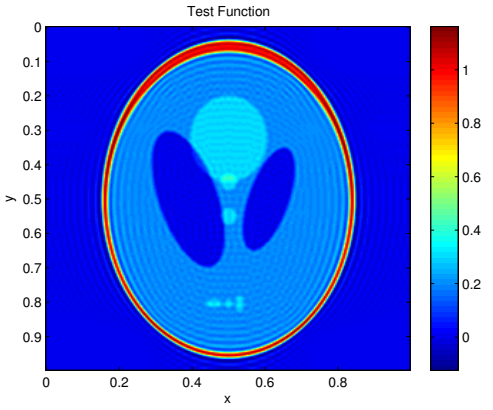

(a) Fourier Reconstruction

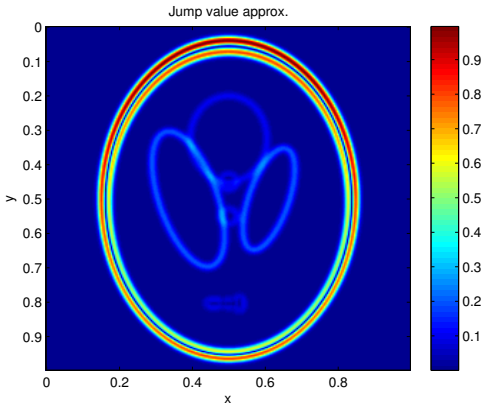

(b) Jump Function Approximation

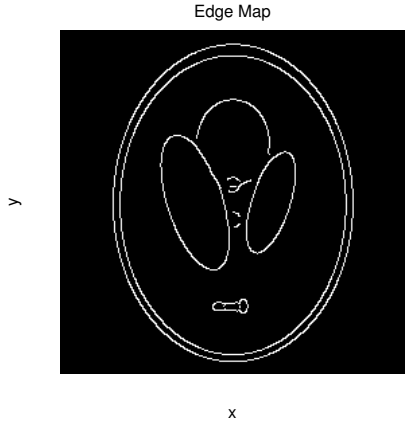

(c) Edge Map

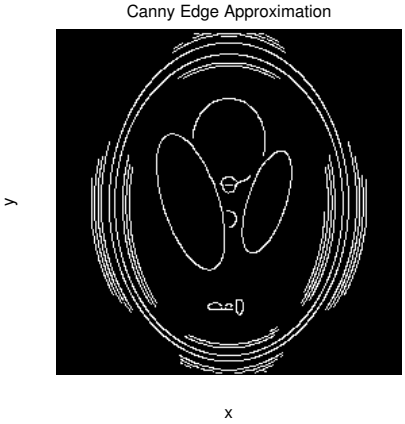

(d) Canny Edge Detector

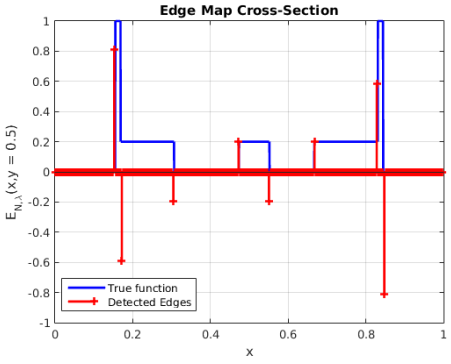

(e) Cross-Section ($y = 0.5$)

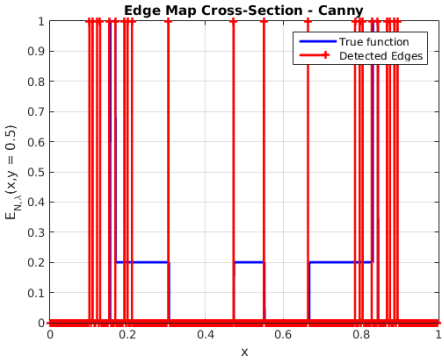

(f) Cross-Section (Canny, $y = 0.5$)

Figure 4: Edge Detection — Shepp-Logan Phantom; $S_N = [-50, 50]^2 \cap \mathbb{Z}^2$ while the equispaced reconstruction grid is of size 256×256 in $[0, 1]^2$.

first 50×50 Fourier modes. Low-resolution measurement acquisitions such as this are common in MR imaging applications For reference, the partial Fourier sum reconstruction (showing significant Gibbs oscillations) is plotted in Figure 4a. Applying the proposed spectral mollifier, the resulting jump funtion approximation is shown in Figure 4b, while the resulting edge map is shown in Figure 4c. Hysteresis edge tracking (similar to that implemented in the Canny edge detector) was used to obtain Figure 4c from Figure 4b. For comparison, we also plot in Figure 4d the results of applying the standard Canny edge detector. Note the presence of a significant number of false positives (see also Figures 4e and 4f for cross-section plots) — these are due to the Gibbs oscillations being spuriously identified as edges by the Canny algorithm. Finally, we note that the proposed method also provides approximations to the jump height (as illustrated in Figure 4e) which may be useful in certain applications such as the solution of PDEs.

Next, we present a higher resolution example in Figure 5, where the edges in the Shepp-Logan are identified starting with the first 200×200 Fourier modes. As before, the results are plotted on a 256×256 equispaced grid. Figure 5a plots the Fourier partial sum reconstruction for reference while Figure 5b plots the jump function approximation. Figures 5c and 5d plot the edge maps generated by the proposed method and the Canny edge detector respectively, while Figures 5e and 5f show the corresponding cross-section plots. In this case, Gibbs oscillations in the Fourier reconstruction are localized to regions close to the true edge locations. Moreover, the standard Canny edge detector does a good job of recognizing and suppressing spurious Gibbs oscillations from true edges. However, note that some of the closely spaced edges are either missing or spuriously identified by the Canny edge detector (see the cross- section plots for an illustration), while the proposed method accurately identifies these.

Figures 4 and 5 have illustrated the performance of the method when we have perfect (noiseless) measurements. We now consider the case where the Fourier modes are corrupted by additive (complex) Gaussian noise; i.e.,

$$\hat{g}(\mathbf{z}) = \hat{f}(\mathbf{z}) + \hat{n}(\mathbf{z}), \quad \mathbf{z} = (z_1, z_2) \in S_N := [-N, N]^2 \cap \mathbb{Z}^2,$$

where $\hat{f}$ an $\hat{g}$ denote the true and noise corrupted Fourier coefficients respectively, and $\hat{n}$ denotes additive noise in Fourier space. In Figure 6, the first 50×50 Fourier modes of the Shepp-Logan phantom are corrupted by i.i.d. additive complex Gaussian noise of variance $\frac{1}{2N^2} = 2 \times 10^{-4}$. The equivalent PSNR is

$$\text{PSNR (dB)} = 20 \log_{10} \frac{\text{max. image intensity}}{\sqrt{\text{Mean Square Error}}} = \frac{\max_{i,j} |f(x_i, y_j)|}{\sqrt{\dfrac{1}{M_x M_y} \displaystyle\sum_{i=0}^{M_x - 1} \sum_{j=0}^{M_y - 1} \left[S_N f(x_i, y_j) - S_N g(x_i, y_j) \right]^2}},$$

where M_x, M_y are the number of points in the reconstruction grid ($M_x = M_y = 256$ in Figure 6) and $S_N f, S_N g$ are the Fourier partial sum reconstructions of f and g respectively:

$$S_N f(x, y) = \sum_{\mathbf{z} \in \mathbf{S_N}} \hat{f}(\mathbf{z}) e^{2\pi i (z_1 x + z_2 y)}, \qquad S_N g(x, y) = \sum_{\mathbf{z} \in \mathbf{S_N}} \hat{g}(\mathbf{z}) e^{2\pi i (z_1 x + z_2 y)}.$$

As before the jump function approximation, edge maps using the proposed method and the

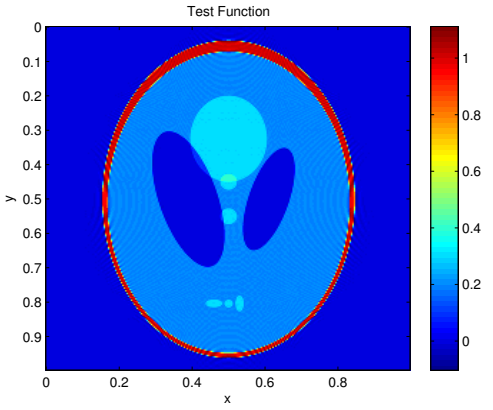

(a) Fourier Reconstruction

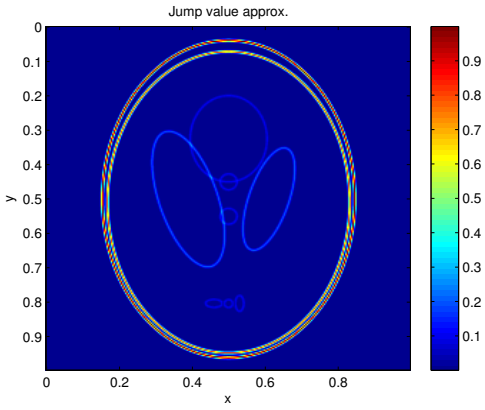

(b) Jump Function Approximation

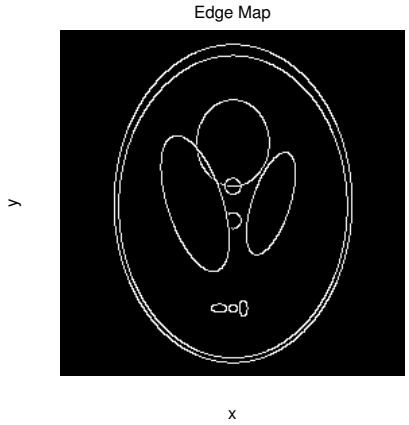

(c) Edge Map

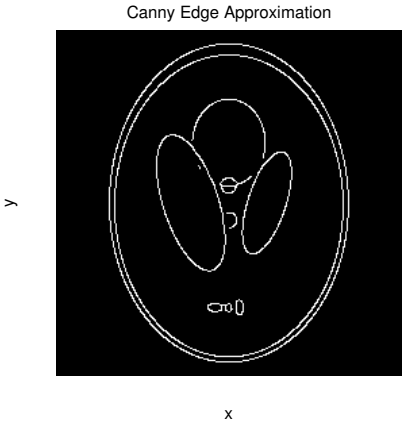

(d) Canny Edge Detector

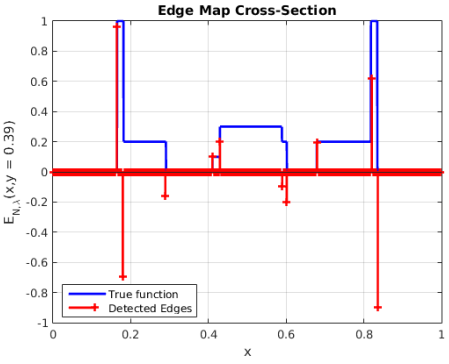

(e) Cross-Section ($y = 0.39$)

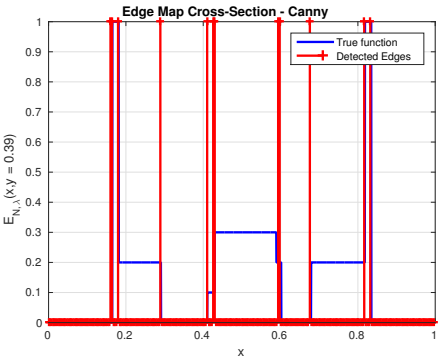

(f) Cross-Section (Canny, $y = 0.39$)

Figure 5: Edge Detection — Shepp-Logan Phantom; $S_N = [-200, 200]^2 \cap \mathbb{Z}^2$ while the equispaced reconstruction grid is of size 256×256 in $[0, 1]^2$.

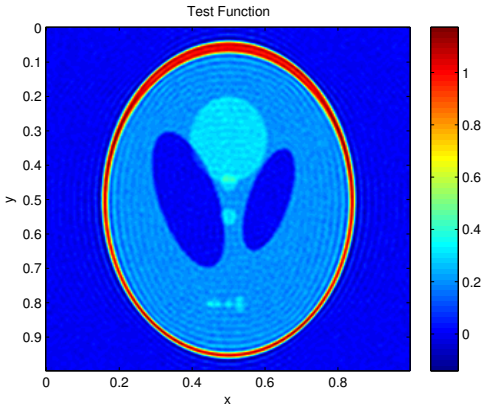

(a) Fourier Reconstruction

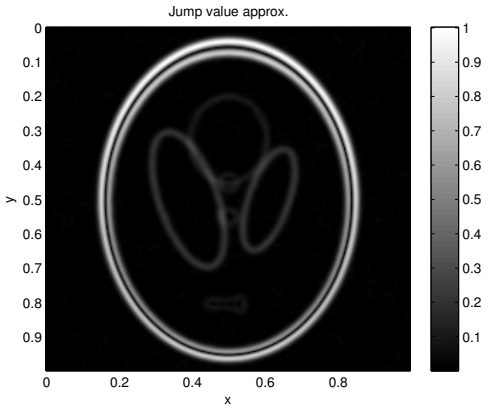

(b) Jump Function Approximation

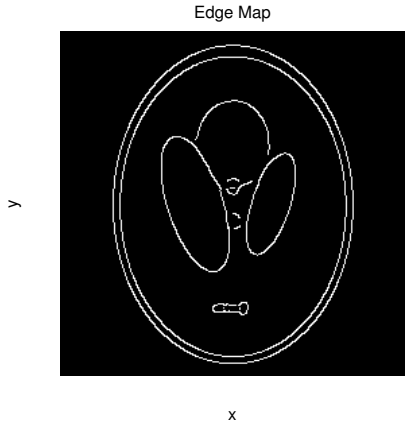

(c) Edge Map

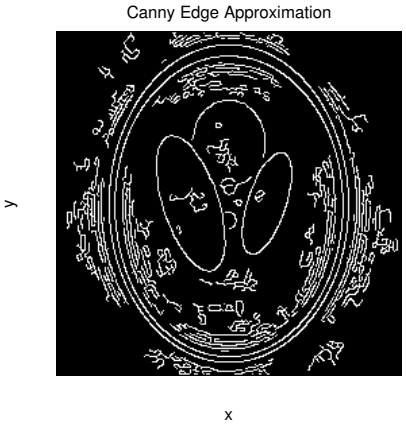

(d) Canny Edge Detector

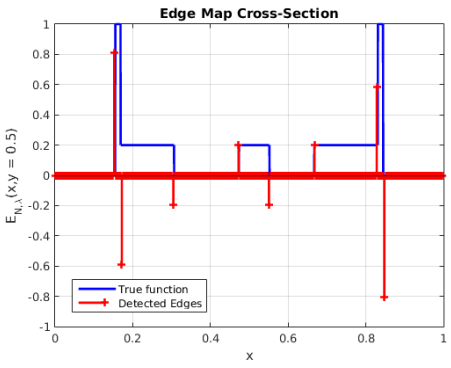

(e) Cross-Section ($y = 0.5$)

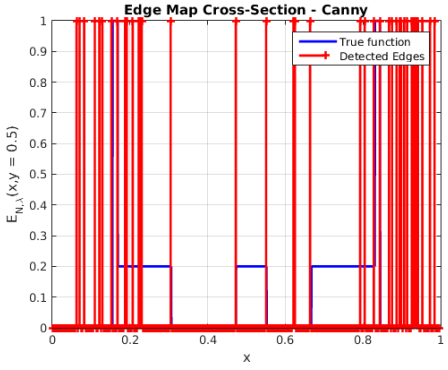

(f) Cross-Section (Canny, $y = 0.5$)

Figure 6: Noisy Edge Detection — Shepp-Logan Phantom; $S_N = [-50, 50]^2 \cap \mathbb{Z}^2$ while the equispaced reconstruction grid is of size 256×256 in $[0, 1]^2$. Additive complex white Gaussian noise of variance 2×10^{-4} (PSNR 36.93 dB) was added to the Fourier modes.

Canny edge detector, and the cross sections of the edge maps are shown in Figures 6a – 6f respectively. We observe that the addition of noise to pre-existing Gibbs oscillations results in the Canny edge detector generating numerous spurious edges, while the proposed method suppresses almost all of these artifacts and generates a near-perfect edge map.

5 Concluding Remarks

In this paper, we have introduced a class of spectral mollifiers for the detection of edges from two-dimensional truncated Fourier data. Recall that the problem of detecting edges from Fourier spectral data is different from and more challenging than the problem of detecting edges from pixel data. Indeed, distinguishing between true edges and Gibbs oscillations is a non-trivial task, especially when we start with a small number of (possibly noise corrupted) Fourier coefficients. We have shown through rigorous analysis that the jump approximations generated using the proposed spectral mollifier are guaranteed to be free of spurious oscillations and edges. Numerical results show that the resulting edge maps are accurate and outperform standard methods such as the Canny edge detector, especially in cases where we have truncated and/or noisy data.

Several interesting avenues for future research exist, including the extension of these results to the case of non-harmonic Fourier data, investigation of the performance of this method for highly incomplete or interrupted data, and the extension of the method to the case of distributed data acquisition.

References

[1] Rafael C. Gonzales and Richard E. Woods. *Digital Image Processing*. Prentice Hall, 3rd edition, 2007.

[2] Jan S. Hesthaven, Sigal Gottlieb, and David Gottlieb. *Spectral Methods for Time-Dependent Problems*. Cambridge University Press, 2007.

[3] Ami Harten, Bjorn Engquist, Stanley Osher, and Sukumar R. Chakravarthy. Uniformly high order accurate essentially non-oscillatory schemes, III. *Journal of Computational Physics*, 71(2):231–303, 1987.

[4] Xu-Dong Liu, Stanley Osher, and Tony Chan. Weighted essentially non-oscillatory schemes. *Journal of Computational Physics*, 115(1):200–212, 1994.

[5] John Canny. A computational approach to edge detection. *Pattern Analysis and Machine Intelligence, IEEE Transactions on*, PAMI-8(6):679–698, 1986.

[6] Doug Cochran, Anne Gelb, and Yang Wang. Edge detection from truncated Fourier data using spectral mollifiers. *Advances in Computational Mathematics*, 38(4):737–762, 2013.

[7] Anne Gelb and Eitan Tadmor. Detection of edges in spectral data. *Applied and Computational Harmonic Analysis*, 7(1):101–135, 1999.

[8] Anne Gelb and Eitan Tadmor. Detection of edges in spectral data II. Nonlinear enhancement. *SIAM Journal on Numerical Analysis*, 38(4):1389–1408, 2000.

[9] Anne Gelb and Eitan Tadmor. Adaptive edge detectors for piecewise smooth data based on the minmod limiter. *Journal of Scientific Computing*, 28(2–3):279–306, 2006.

[10] Eitan Tadmor and Jing Zou. Three novel edge detection methods for incomplete and noisy spectral data. *Journal of Fourier Analysis and Applications*, 14(5–6):744–763, 2008.

[11] Anne Gelb and Dennis Cates. Detection of edges in spectral data III – Refinement of the concentration method. *Journal of Scientific Computing*, 36(1):1–43, 2008.

[12] Alex Petersen, Anne Gelb, and Randall Eubank. Hypothesis testing for Fourier based edge detection methods. *Journal of Scientific Computing*, 51(3):608–630, 2012.

[13] Adam Martinez, Anne Gelb, and Alexander Gutierrez. Edge detection from non-uniform Fourier data using the convolutional gridding algorithm. *Journal of Scientific Computing*, 61(3):490–512, 2014.

[14] Anne Gelb, Guohui Song, Aditya Viswanathan, and Yang Wang. GiFtED: Matlab software for Gibbs-Free Edge Detection, version 1.0. `https://bitbucket.org/charms/gifted`, 2015.